AIAA JOURNAL
Vol. 46, No. 9, September 2008

Flow Control by Dielectric Barrier Discharge Actuators: Jet Mixing Enhancement

N. Benard,* J. P. Bonnet,† G. Touchard,‡ and E. Moreau§
Université de Poitiers, 86962 Futuroscope Cedex, France

DOI: 10.2514/1.35404

This study is focused on a new approach to control the mixing at the exhaust of a jet nozzle. Two dielectric barrier discharges are used to enhance the turbulent quantities in the jet wake. An axisymmetric air jet is equipped with a 22-degree-angle diffuser that houses two dielectric barrier discharge actuators, symmetrically placed along the lips of the diffuser. Streamwise, cross-stream planes, and turbulent spectra for free air jet velocities from 10 to 40 m/s are investigated by stereoscopic particle image velocimetry and laser Doppler velocimetry up to 8 jet diameters. The airflow is separated naturally along the diffuser wall and the results demonstrate that a full (at 10 m/s) or partial (at 20 m/s) flow reattachment can be performed, this process being associated with the shedding of coherent structures. The turbulent spectra suggest that the frequency of the vortex shedding is dictated by the electrical frequency applied to the actuators and that the flow structures can be manipulated up to 40 m/s. The time-averaged data confirm that a significant enhancement of the jet spreading, a jet core length reduction, and a turbulent kinetic energy increase are performed up to 30 m/s for a quasi-steady actuation. Unsteady actuations are also investigated and the results highlight that a Strouhal number from 0.25 to 0.32 is particularly effective to enhance the turbulent kinetic energy in the overall flowfield.

Nomenclature

D	=	internal nozzle diameter
d	=	exhaust diameter
d_{droplets}	=	size of the seeding particles
f	=	electrical frequency
h	=	height of the turbulator ring
k	=	turbulent kinetic energy
Re_D	=	Reynolds number based on internal nozzle diameter D
St	=	Strouhal number (jet column mode), $St = fD/U_j$
St_θ	=	Strouhal number computed on the momentum thickness, $St_\theta = f\theta/U_j$
t	=	time
U_c	=	convective velocity
U_j	=	primary air jet velocity
u_x	=	streamwise velocity component
u_y	=	cross-stream velocity component
u'_x	=	primary component of the fluctuating velocity
u'_y	=	secondary component of the fluctuating velocity
δ_w	=	vorticity thickness
$\delta_{1/2}$	=	jet width
θ_0	=	initial momentum thickness

Received 31 October 2007; revision received 5 May 2008; accepted for publication 5 May 2008.

*Research Assistant, Laboratoire d'Etudes Aérodynamiques Unite Mixte Recherche 6609, Boulevard Marie et Pierre Curie. AIAA Member.

†Research Director, Laboratoire d'Etudes Aérodynamiques Unite Mixte Recherche 6609, Centre d'Etudes Aérodynamique et Thermique, Boulevard Marie et Pierre Curie. AIAA Member.

‡Professor Emeritus, Laboratoire d'Etudes Aérodynamiques Unite Mixte Recherche 6609, Boulevard Marie et Pierre Curie.

§Professor, Laboratoire d'Etudes Aérodynamiques Unite Mixte Recherche 6609, Boulevard Marie et Pierre Curie.

I. Introduction

THE control of the wake of axisymmetric jet flow has strong implications for a wide variety of practical flows. The control of such flow primarily concerns military applications but also has environmental implications. Military fighters and rocket engines require a rapid mixing of the exhaust jet to enable a more rapid reduction in the temperature, thus limiting the strongest infrared radiations [1]. However, environmental regulations or penalties imposed to the civil companies should be more stringent in the future. The commercial engines thus need to reduce emissions of pollutants and unburned fuel and require to limit the radiated noise. Consequently, the flow through a gas-turbine combustor involving round reactive jets also requires an adaptive control. An increase of the mixing allows the engine to burn the remaining fuel, and generally requires it to spread the jet, as opposed to the reduction of CO emission, which consists of increasing the particle residence time via a decrease of the mixing [2]. Other applications at lower velocity concern civil engineering, such as pollutant dispersion of power plant chimneys.

Jet flow control generally consists in modifying the geometry or the exit conditions of jets to promote turbulent mixing closer to the air jet exit. Active and passive controls present a common goal which consists of manipulating the scales of the turbulent structures. Indeed, the mixing layer between two fluids with different velocities, temperatures, or densities is naturally unstable. Thus, small perturbations imparted to the flow structures can be strong enough to lead to a significant change in the mixing properties, and the mixing rate of a turbulent jet can be significantly altered by applying a suitable excitation at the jet exit. As demonstrated by the use of chevrons, fluidic chevrons, fluid injection, acoustic excitation, or tab configurations, for example [3–7], the turbulent kinetic energy in the near-field region (in which the coherent structures prevail) can be increased. As previously mentioned, the initial shear layer of axisymmetric jets is sensitive to small disturbances, which under certain conditions are amplified through their natural instability [8], and a large spreading can be achieved if suitable excitation frequencies are chosen [9]. Unsteady excitations at strategic locations are an efficient control strategy to largely modify the near-exit of air jets. In this context, plasma actuators appear to be a promising alternative to mechanical and fluidic control devices. The increasing popularity of the nonthermal surface plasma actuators is evidenced by the diversity of their applications in flow control [10,11]. Flow separation and reattachment on airfoils [12,13],

control of vortex shedding at cylinder edges [14,15], or delay of the boundary-layer transition [16] can be achieved using surface plasma actuators. The surface plasma generated by a dielectric barrier discharge (DBD) system induces a local velocity of a few meters per second [17–19]. This nonmechanical device produces electrofluidodynamic (EFD) forces induced by applying a high voltage (HV) between two electrodes insulated by a thin dielectric material. Contrary to the arc filament plasma actuator developed by Samimy et al. [20], the EFD forces produced by a surface DBD are located a few millimeters above the dielectric wall and directly interact in the wall shear layer without thermal implication. Actuators based on this technology are suitable for the control of an axisymmetric air jet, as previously demonstrated by Corke and Matlis [21]. The authors used phased plasma arrays composed of nine DBDs to control a subsonic axisymmetric air jet. The plasma formed in contact with the air jet allowed the authors to excite the helical modes. The results demonstrated that actuation induced higher centerline fluctuations and that, downstream of the jet exit, the excitation resulted in a faster centerline velocity decay, demonstrating an increase in mixing. More recently, the authors have demonstrated that a jet vectoring of 13.5 deg can be performed using a single DBD actuator located at the exit of a 12-deg-angle diffuser nozzle, thus promoting nonsymmetric actuation resulting in a deviation of the main jet [22].

In the present study, an axisymmetric nonreactive turbulent air jet is controlled using two DBD actuators placed symmetrically at the surface of a 22-deg-angle diffuser. Steady and unsteady actuations are investigated to define the most efficient excitation mode to enhance the large vortex structures and the increase in mixing. The results are obtained using a stereoscopic particle image velocimetry system, allowing one to measure the two or three velocity components in the near-field region. The flowfield inside the nozzle is also investigated. Complementary data acquisitions are performed using a laser Doppler velocimetry system, allowing one to compute the spectral energy density spectra along the shear layer centerline. The analysis is based on the flow modifications in the longitudinal and streamwise planes. Further analyses are performed by examining the turbulent kinetic energy values and the power spectra density.

II. Experimental Setup

A. Experimental Setup: The Jet Facility

An initially turbulent round jet with a centerline velocity up to 40 m/s is investigated in the present study. This air jet is produced by a circular open wind tunnel (diameter of 400 mm and length of 2 m) in which the flow is driven by a variable frequency centrifugal fan (FEVI F18G-1R-500). To obtain homogenous flow conditions, the air entrained by the centrifugal fan passes through a series of five fine screens with decreasing grid sizes before entering into the contraction and the jet nozzle. The section of the wind tunnel is reduced by the use of a contraction outlet having a section ratio of 1:64. Finally, the flow has an internal diameter D of 50 mm upstream of the diffuser. A 22-deg-angle diffuser is housed inside the jet nozzle and, according to the 30-mm-long bevel, the resulting exhaust diameter d is 72.5 mm, as illustrated in Fig. 1a. The Reynolds numbers Re_D, based on the internal jet diameter D, range from 33,000 to 128,000. The aerodynamic configuration and the primary jet velocity lead to classical uniform top-hat velocity profiles at the jet exit and the flow is naturally detached from the beveled walls. The main idea of this study is to design an actuator suitable for mixing enhancement using a forced flow reattachment along the bevel or by exciting the flow where instabilities initiate. Practical flows are usually fully turbulent. However, laminar flows are often preferred in academic research. Then, laminar-to-turbulent transition may be suspected to be responsible for the control observed. In the present study, the axisymmetric jet is initially fully turbulent by the use of a tripper ring made of aluminum oxide ($h = 350\ \mu$m) located $4D$ (200 mm) upstream of the diffuser exhaust. The use of the turbulator ring results in a peak fluctuation level of 17.8% upstream of the diffuser at 40 m/s and 14.6% at 10 m/s, whereas the turbulence level in the core of the jet is about 6%.

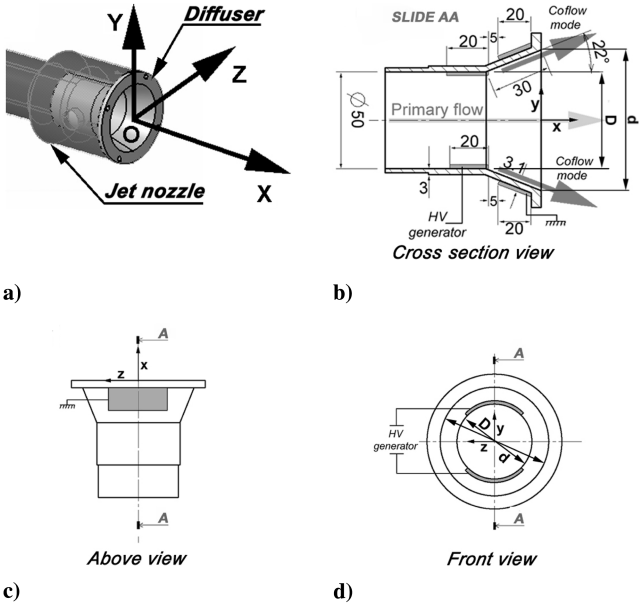

Fig. 1 Housed diffuser and actuator design: a) schematic, b) cross-sectional view, c) above view, and d) front view.

B. Description of the Dielectric Barrier Discharge Actuator

According to the characteristics established by Forte et al. [23] for an optimization of the EFD forces produced by a single DBD actuator, the electrodes are 20 mm wide and 40 mm long. The plasma discharge region is extended by the use of a small gap of 5 mm between the electrodes. Contrary to synthetic jets, which require small holes at the body surface modifying the boundary-layer properties, the electrodes of the DBD actuator are sufficiently thin (0.1 mm) to avoid flow disturbance and associated thrust loss. The jet nozzle and housed diffuser are made of polymethyl methacrylate to avoid electrical interactions, and the thickness of the diffuser acts as a thin (3 mm) dielectric barrier surface, as shown in Fig. 1b. The electrodes of the actuator are made of aluminum sheets stuck on the diffuser surface (the active electrode corresponds to the air-exposed one, whereas the grounded electrode is the insulated one). The DBD configuration produces a coflow EFD force, and two DBD actuators are placed symmetrically on the nozzle wall to excite both sides of the diffuser. The electrodes cover 50% of the jet perimeter, as illustrated in Figs. 1c and 1d.

A sine signal generated by a digital waveform synthesizer is amplified by a high-voltage power generator (Trek 30 kV/40 mA, New York). The air-exposed electrode is supplied by a 40 kVpp (peak to peak) at a 1.5 kHz frequency, resulting in a total electric consumption of 9.6 W when operating in quasi-steady mode. In a previous study using similar electrode and electrical configurations, the measurement of the produced "electric wind" by a pitot tube made of glass has demonstrated that the time-averaged airflow reaches 6 m/s (at 0.5 mm from the wall) tangentially to the dielectric wall [22]. This measurement was performed for a 12-deg-angle diffuser, but it could be expected that the change in angle does not interact with the maximal value of the electric wind. This electric wind is due to the momentum transfer from the ionized particles to the neutral atmospheric air component. The nonthermal plasma device can be operated either in a quasi-steady or unsteady manner. The quasi-steady mode consists of applying the electrical signal detailed earlier. This kind of actuation can be named "quasi steady" because the fluid response of the flow is supposed to be much lower than the ac frequency. In the unsteady actuation mode, a first signal at 1.5 kHz is alternatively switched off and on at a lower frequency [24]. The number of sine wave periods is defined to set the unsteady actuation at a duty cycle maintained constant at 50%, as shown in Fig. 2.

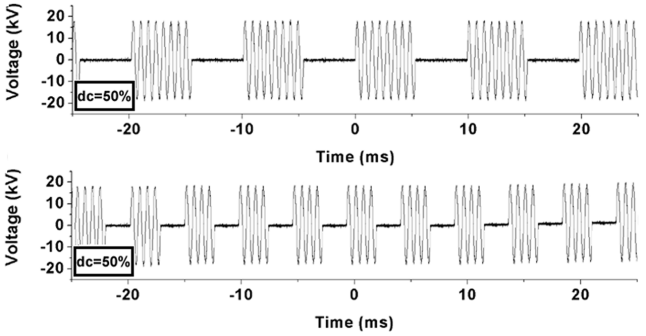

Fig. 2 Illustration of unsteady excitations at a duty cycle fixed at 50% and modulating low frequency of a) 100 Hz, and b) 200 Hz.

C. Flow Diagnostic Setup

The velocity components u_x and u_y in the wake region of the jet flow are measured by a typical particle image velocimetry (PIV) system, whereas the three velocity components are acquired by a stereoscopic-PIV arrangement for measurements in the cross-stream plane and inside the diffuser. The PIV systems are composed of one or two charge-coupled device (CCD) cameras (Lavision, 1376×1040 pixels) and a Nd:Yag laser. Each laser head operates at 27 mJ per pulse and a 1-mm-thick laser sheet is adjusted by the use of lenses. The camera and the Nd:Yag laser are operated at a frequency of 4 Hz. The flow is seeded using oil droplets ($d_{\text{droplets}} = 0.5$–$2\ \mu$m) atomized by a smoke generator (Deltalab, EI511) and injected in the centrifugal fan. A cross-correlation algorithm with adaptive multipass, interrogation windows of 32×32 to 16×16 pixels, and an overlap set to 50% is applied to the digital couples of images to compute the instantaneous vector fields. The time-averaged and turbulent quantities are calculated from 300 instantaneous fields. Standard bidimensional PIV is used to investigate the u_x and u_y velocity components of the flowfield occurring in the longitudinal planes (planes OXY, in Fig. 1a). As shown in Fig. 3a, the laser sheet and digital camera axis are perpendicular, whereas the CCD camera is mounted at a distance of 0.5 m from the laser light sheet. The laser is adjusted at $z/D = 0$ and, according to the distance between the lighted plan and the camera, the resulting spatial resolution of the vector fields is 1.74×1.74 mm^2. The acquisition of the velocity field in the cross-stream plane is performed by the use of a stereoscopic-PIV system operating in backward scattering mode, as illustrated in Fig. 3b. The CCD cameras are mounted downstream of the laser sheet and they are equipped with a Scheimpflug adaptor to reduce optical aberrations. An opening angle of 90 deg between the cameras is retained to minimize errors on the primary velocity component u_x. Cross-stream acquisitions are realized at 5 mm of the jet exit ($x/D = 0.1$) and the field of view is $-0.9 < x/D < 0.9$ and $-0.9 < y/D < 0.9$. Because of a higher scale factor, the spatial resolution is increased comparatively to the streamwise plane and it reaches 0.097 mm per pixel. The flow is analyzed by cross correlations with overlapping windows of 32×32 pixels performed on 300 couples of two images. For the last PIV measurements (see Fig. 3c), the arrangement of both cameras and the laser allows one to measure the flow at the bevel wall, inside the diffuser, with minimized wall reflections. The cameras are equipped with a Scheimplug adaptor and with a 50-mm objective lens, resulting in a field of view of 90×50 mm. For these data sets, phase acquisitions are performed by triggering the PIV system with the electrical signal supplied to the actuator. The velocity fields at each phased acquisition are composed of an ensemble averaged of 150 couples of two images (60 ms of actuation is sampled using 12 discrete instants, i.e., each 5 ms). A spatial resolution of 0.8×0.8 mm^2 is reached by cross correlating the images with 50% overlapping of 32×32 windows. To minimize the experimental time, the quasi-steady actuations are investigated up to 40 m/s, but the extensive study of the effects of the Strouhal number is voluntarily limited to two intermediate velocities of 20 and 30 m/s.

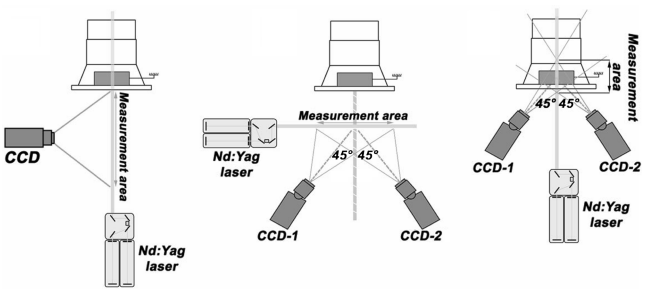

a) b) c)

Fig. 3 Laser sheet and digital camera arrangements for a) streamwise acquisitions, b) cross-stream acquisitions, and c) measurements along the diffuser bevels.

Complementary measurements using a laser Doppler velocimeter (LDV) system are performed to characterize the turbulent energy of the flow structures in the shear layer for primary air jet set to 20 m/s only. The light source (5 W Argon-ion laser) produces blue and green beams (wavelengths of 488 and 514 nm, respectively) which compose a probe volume of 0.2×3 mm^2. The optics are arranged in a ± 45 deg configuration, which increases the accuracy of the tensor Reynolds components [25]. To precisely define the spatial location of the probe volume, the LDV system is mounted on a micrometric displacement system (± 0.01 mm). The sampling frequency varies between 10 and 20 kHz and 10^6 bursts are collected. A flow velocity analyzer (Dantec) discards the wrong velocities and extracts the time-stochastically sampled velocities. Data are collected for height locations along the shear layer centerline for natural and forced airflows. The shear layer centerline is defined as the position at which velocity is half of the maximal cross stream. By nature, the velocity signal resulting from LDV is intermittent with a random arrival of particles. To overcome this characteristic, the fuzzy slotting technique and the local normalization approach are combined (see van Maanen et al. [26] for details) to significantly increase the power spectra estimation.

D. Bias Error and Measurements Accuracy

Although advanced measurements systems such as PIV and LDV have demonstrated their ability to study laminar and turbulent flows, the accuracy of the obtained results needs to be addressed, in particular, when the natural or forced flow changes are low.

For PIV acquisitions, the accuracy of the vector fields depends on parameters such as particle size and density, loss of particle in lighted laser plane, or high velocity gradient. The influence of these parameters on the measurements precision requires specific experiments or theoretical estimations and, unfortunately, cannot be estimated from the present data sets. However, some indicators can furnish relevant information about the global quality of the experiment. For instance, in the present study, a local median filter is used to detect and remove the spurious vectors. The confidence in the obtained results is rather high, even if a detailed analysis of the rejected vectors in the PIV fields demonstrates that some image sequences lead to an increase of the number of rejected vectors. An analysis of these instantaneous velocity vectors reveals that the higher percentage of rejected vectors over an entire acquisition sequence is lower than 6.5%. The location of the spurious vectors is mainly concentrated at the airfoil surface. When these surrounding regions are discarded from the analysis, the higher level of spurious vectors is lower than 2%.

Another point is the statistical convergence of the time-averaged quantities as the acquisition is performed over a finite number of samples. The 2-D and stereoscopic-PIV acquisitions related to the characterization of the jet wake are composed of 300 pairs of images, as previously described. The statistical analysis of the first- and second-order time-averaged values confirms that mean quantities are well converged when a minimal numbers of samples are used. At 10 m/s, the results confirm that all the velocities are converged if 200 PIV fields are used, at least. At higher velocity, the number of samples required to obtain a satisfactory convergence is increasing,

Table 1 Uncertainty on mean flow and Reynolds stress components computed by a 95% confidence interval for 2-D streamwise PIV

Sensor 1	10 m/s	20 m/s	30 m/s	40 m/s
$\overline{u}_x$	0.0015	0.0058	0.0203	0.0619
$\overline{u}_y$	0.0008	0.0029	0.0069	0.0171
$\overline{u_x^2}$	0.0006	0.0076	0.0629	0.7981
$\overline{u_y^2}$	0.0002	0.0025	0.0141	0.1013
$\overline{u_x}\,\overline{u_y}$	0.0002	0.0039	0.0234	0.1881
Sensor 2	10 m/s	20 m/s	30 m/s	40 m/s
$\overline{u}_x$	0.0059	0.0292	0.0610	0.1710
$\overline{u}_y$	0.0043	0.0191	0.0545	0.1082
$\overline{u_x^2}$	0.0099	0.4978	1.4177	11.9015
$\overline{u_y^2}$	0.0054	0.1296	0.9608	3.5365
$\overline{u_x}\,\overline{u_y}$	0.0051	0.1770	0.6577	3.8120
Sensor 3	10 m/s	20 m/s	30 m/s	40 m/s
$\overline{u}_x$	0.0077	0.1550	0.0682	0.1815
$\overline{u}_y$	0.0013	0.0152	0.0365	0.0860
$\overline{u_x^2}$	0.0247	3.2654	1.6784	13.1205
$\overline{u_y^2}$	0.0032	0.1519	0.3798	2.3313
$\overline{u_x}\,\overline{u_y}$	0.0060	0.6721	0.4421	3.6798

but it appears that 250 samples are sufficient to reach a stabilized convergence rate of about 98%. The measurement of the u_x velocity component by stereoscopic PIV for cross-stream acquisition is more sensitive to bias error due to higher drift value and possible integration over the laser sheet thickness. The comparison of the intersecting section between the streamwise and cross-stream planes reveals that the error on the u_x component is approximately 6% when stereoscopic PIV is used. For the phased acquisitions, the number of samples is decreased to reduce the time of the experiment (150 couples of two images are collected). However, the velocity components u_x and u_y are converged using only 40 couples of images.

As described by Benedict and Gould [27], a way to define the uncertainties on turbulent quantities consists of computing a confidence interval for the sample mean. In the present study, a confidence interval of 95% is chosen and the results, in terms of dimensionalized uncertainty, is illustrated in Table 1 for the 2-D PIV setup (results are similar with other PIV arrangements). The results confirm an acceptable accuracy for velocity measurements in the potential core (sensor 1 in Fig. 4), beyond the end of the potential core (sensor 2 in Fig. 4) and in the free shear layer region (sensor 3 in Fig. 4). An increase of uncertainty is observed for the Reynolds stress component at 40 m/s, but the results remain fully valid because the relative uncertainty is equal to 0.8%.

Other bias errors are directly related to the hardware and velocity field computation setup of the PIV acquisition. In the present study, multipass cross correlations are used to compute the particle displacement over the field of view. This algorithm results in a subpixel error, which means that the displacement of each particle is estimated with an accuracy of about 0.1 pixel. By taking into account the scale factor, the subpixel bias error on the displacement, and the time between two successive images, it becomes feasible to estimate the uncertainty of each instantaneous velocity at each investigated primary airflow speed, as summarized in Table 2.

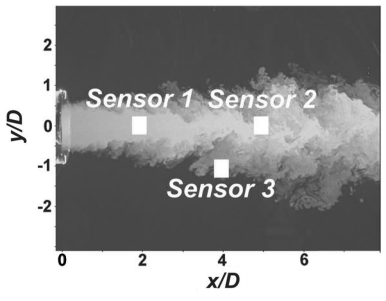

Fig. 4 Location of the sensors for computation of the uncertainty.

Table 2 Uncertainty on instantaneous velocity due to the detection method for PIV measurements

Streamwise plane, PIV 2-D			
10 m/s	20 m/s	30 m/s	40 m/s
1.18%	1.18%	1.22%	1.22%
Cross-stream plane, stereoscopic PIV			
10 m/s	20 m/s	30 m/s	40 m/s
1.07%	1.07%	1.07%	1.07%
Streamwise plane, stereoscopic PIV			
10 m/s	20 m/s		
0.75%	0.37%		

Among other time-resolved measurement systems, LDV is one of the most accurate. This technique minimizes the bias error on the instantaneous velocities, despite particle averaging or velocity gradient biases whose corrective methods are still debated by the community. Here, the uncertainties are estimated by using a 95% confidence interval. A random drawing of 10.000 instantaneous velocities is realized to base the analysis on independent elements. The 95% confidence interval was found to be of 3.8×10^{-4}, 0.18×10^{-4}, 23.6×10^{-4}, 1.57×10^{-4}, and 25×10^{-4} for $\overline{u}_x$, $\overline{u}_y$, $\overline{u_x^2}$, $\overline{u_y^2}$, and $\overline{u_x}\,\overline{u_y}$, respectively.

The temporal definition of LDV measurements conduces to use such measures for spectra density analysis. Here, the power spectra density is computed by using an advanced algorithm, which has demonstrated its relevancy for supersonic flows and during international benchmark tests [28,29]. The merging of the local normalization and fuzzy algorithm conduces to a decrease of the variance of the individual correlation coefficient, as demonstrated by van Maanen et al. [26]. However, independent of the error produced by the algorithm itself, the presence of uncertainty on fluctuating velocities results in potential errors of the density spectra estimation. To evaluate this bias, one acquisition sequence is weighted by an error factor of 2, 5, and 10%. Each sequence is treated by the same normalized fuzzy algorithm and the resulting power spectra densities are compared. The results reveal that the error on the power spectra density are 3.7, 8.9, and 16% when an original signal is noised by 2, 5, and 10% of error on the mean or fluctuating velocities. Assuming that typical precision of LDV is smaller than 2%, one can expect that the uncertainty of the power spectra density is smaller than 3.7%.

III. Results and Discussion

A. Quasi-Steady Actuation: Flowfields Inside and at the Jet Exit

In this section, the flow profiles along the bevel are introduced. The cross-stream mean velocity profiles at $x/D = 0.1$ are extracted from the 2-D PIV fields. The results shown in Fig. 5 demonstrate that the baseline jet flow is self-similar even a few millimeters downstream of the jet diffuser exhaust. The results in Fig. 5 highlight that a full-forced flow reattachment is only effective for a primary air jet velocity of 10 m/s. The jet width $\delta_{1/2}$, based on the radial position at which the velocity is half of the potential core velocity value, is largely increased with a jet width gain of about 31% and, consequently, highlights the velocity displacement under actuation. Moreover, at $z/D = 0$, the vorticity thickness δ_w, defined as $\delta_w = U_j/(\partial U/\partial y)_{\max}$, has been increased by a factor of 83% ($\delta_{w\mathrm{OFF}} = 0.18D$ and $\delta_{w\mathrm{DBD}} = 0.33D$). Then, the jet spreading is enhanced via an increase of the mixing surface, while the simultaneous increase of the local vorticity thickness could result in a turbulent mixing rise. At 20 and 30 m/s, shown in Fig. 5, a small velocity displacement is observed in the shear layer region (jet width gain of about 5%) while the vorticity thickness kept constant ($\delta_w = 0.18D$), highlighting that only minor flow change occurs at $z/D = 0$. In quasi-steady mode, the EFD forces produced by the DBD actuator operating in steady mode are too small to induce a macroscopic time-averaged flow modification at $z/D = 0$. However, additional measurements could highlight that the actuator's authority

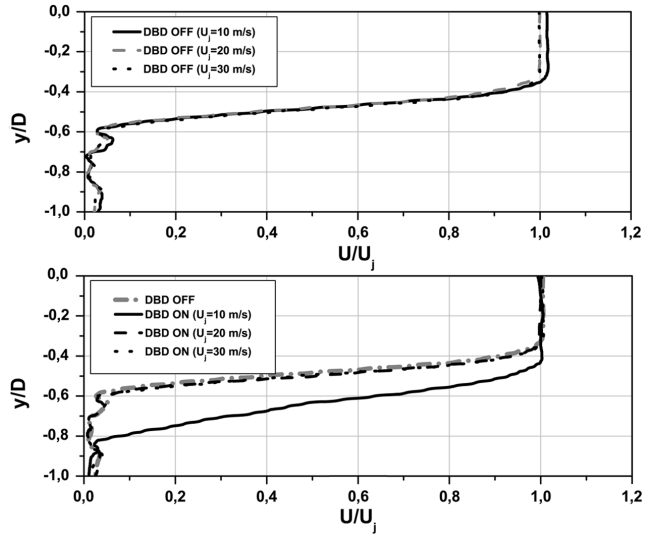

Fig. 5 Mean velocity profiles in the cross-stream direction ($z/D = 0$) at $x/D = 0.1$. (The gray dotted line refers to the mean values of the baseline profiles at 10, 20 and 30 m/s.)

is increased at other z/D positions, as demonstrated in the following parts of the present paper.

The time-averaged phase acquisitions acquired at $U_j = 10$ m/s allow one to understand the full reattachment process at one actuator. Figure 6b presents the flow state at $t = 10$ ms. The formation of a recirculation region is noticeable and may result from the local pressure decrease created by the EFD force. This recirculation grows and rolls along the bevel wall and finally creates a discrete vortex structure at the jet exhaust, seen in Figs. 6b–6e, convected at $U_c = U_j/2$ (approximately at 5 m/s, as expected). The large-scale flow structure is formed within 15 ms. At 20 m/s, shown in Fig. 7, the same separation process occurs, the time necessary to create the large coherent structure is decreased ($t < 10$ ms) and the results confirm that the flow is reattached only on one-third of the bevel length. The convective velocity of this large eddy is now 9 m/s. The reattachment process requires approximately 15 and 10 ms for a primary jet velocity of 10 and 20 m/s, respectively. Contrary to the observations previously published by Gregory et al. for a fluidic oscillator enhanced by a DBD actuator [30], the reattachment time decreases at higher velocity. However, the aerodynamic configuration in this study involves a coflow forcing, and a previous study about the flow separation forced by counterflow actuation has proved that the response time increases at higher velocity [31]. In particular, the separation process is temporally reduced if the electric power is increased [32]. Consequently, the time necessary to initiate the shedding of a coherent structure could be reduced by increasing the electric power consumption. These vortices shedding are important because they result in pressure fluctuations enhancing the shear layer roll up. More, the large structures could intensify the momentum transfer from the jet to the external free shear layer, resulting in mixing enhancement. The vortex shedding is not apparent for a primary velocity greater than 20 m/s, which is in pretty good

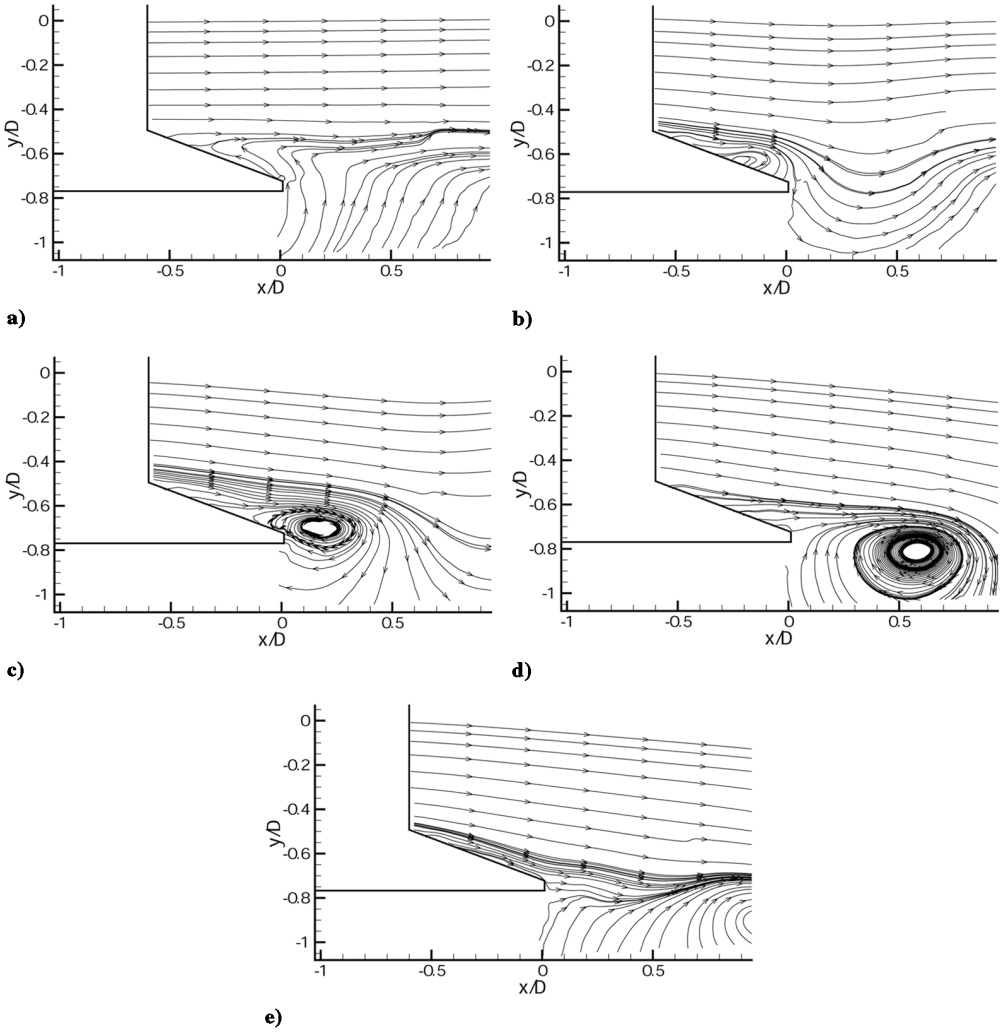

Fig. 6 Phased streamlines of the forced flow attachment at 10 m/s at a) initial actuation time, b) 10 ms, c) 15 ms, d) 20 ms, and e) 25 ms obtained by stereoscopic PIV.

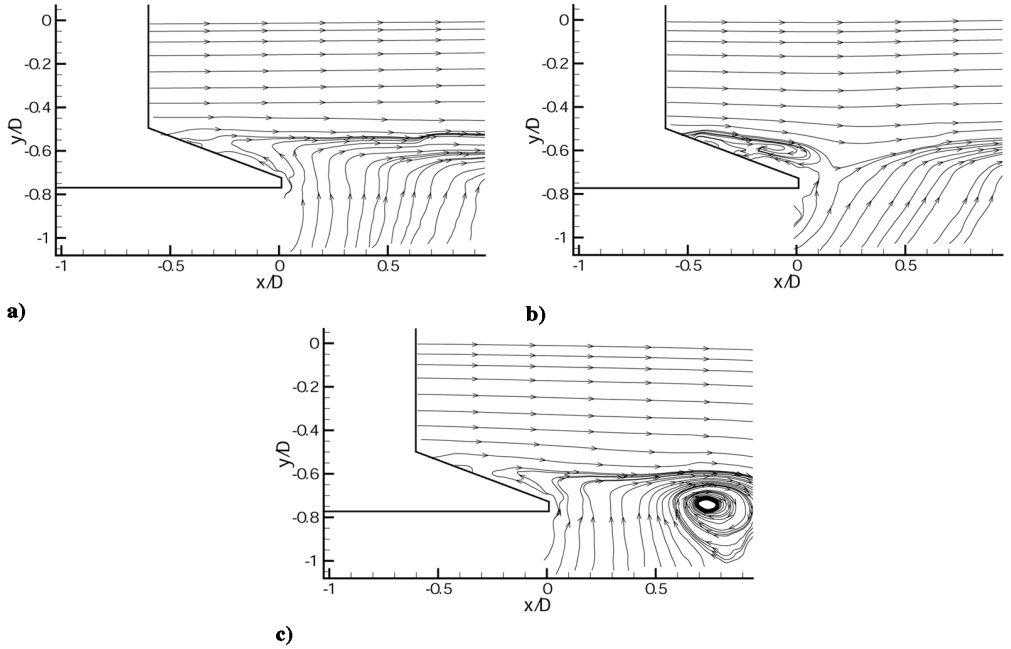

Fig. 7 Phased streamlines of the forced flow attachment at 20 m/s time-averaged at a) initial actuation time, b) 5 ms, and c) 10 ms by stereoscopic PIV.

agreement with the time-averaged velocity profiles. An effective control by plasma actuation could consist of promoting the creation of large-scale structures improving turbulence production or enhancing the mixing by excitation of the natural instabilities initiated in the diffuser. These control strategies require unsteady actuation, which is introduced later in the paper.

B. Quasi-Steady Actuation: Streamwise and Cross-Stream PIV Results in the Near-Field Region

The time-averaged velocity norm computed on streamwise u_x and cross-stream u_y velocity components is plotted in Fig. 8 for the streamwise plane measured by 2-D PIV. The baseline jet (denoted by the gray dotted lines in Fig. 8) is symmetric about the x axis and presents self-similar distribution due to the initially turbulent boundary layer. Following the double DBD actuation (indicated by the black lines in Fig. 8), major macroscopic flow changes appear for a primary air jet of 10 m/s. The spreading is largely increased in the first diameters (up to $x/D = 2$), followed by a region of quasi-parallel flow associated with a lower jet spreading. For air jets from 20 to 40 m/s, the EFD forces created by the plasma are too weak to force the flow reattachment, but the jet presents a slightly larger spreading in the wake, up to $U_j = 40$ m/s.

To qualify the velocity distribution in the cross-stream plane, the time-averaged norm measured by stereoscopic PIV is plotted in Fig. 9 for a yz plane at $x/D = 0.1$. As expected, the baseline cross-stream fields spread in concentric circles of uniform velocity. Under actuation, the flow at $U_j = 10$ m/s is deflected toward the bevels at which the actuators act, causing the velocity profiles to elongate. The jet cross section contracts in the x direction and expands in the y

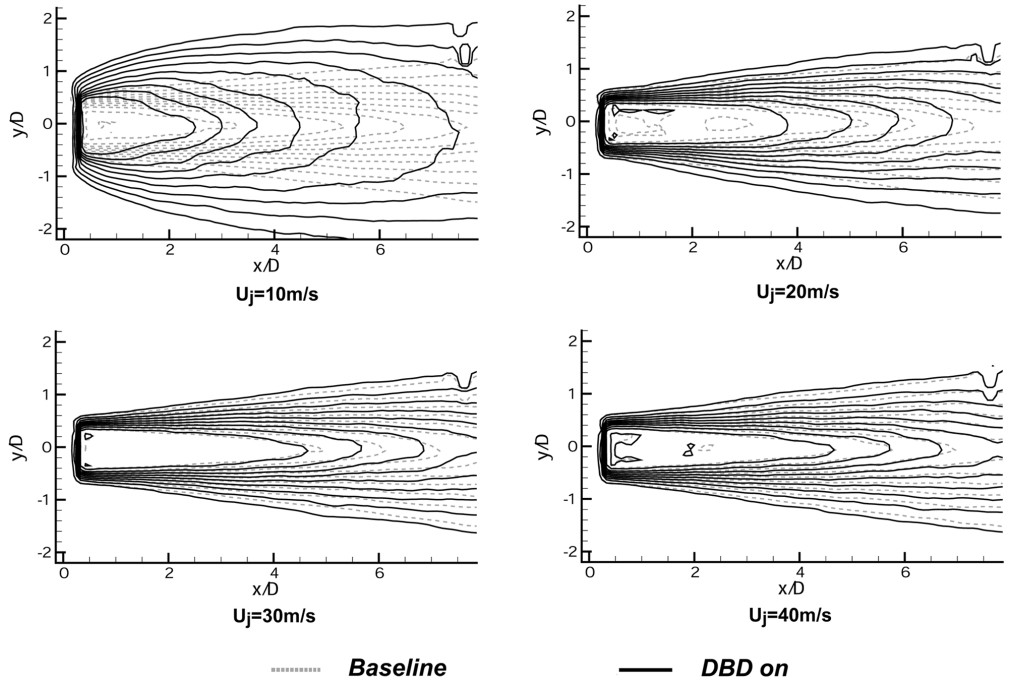

Fig. 8 Time-averaged velocity norms for the axial plane. The isovelocity contours have increasing values toward the exit (from 0 m/s up to U_j).

direction, as previously observed by other authors using a blowing jet located at the nozzle exit [7,33]. One can notice that Fig. 9 confirms the increase in vorticity thickness in the y direction, although the x direction is not affected. For a freestream velocity of 20 m/s, the flow remains moderately elongated. In particular, the cross section is modified at the corners of the actuators. At these corners, the vorticity thickness is increased (mean vorticity thickness gain of about 47% at each corner). The mixing enhancement could thus be related to the small increase of the interface of the outer and inner fluids combined with the vorticity thickness gain at the corners. At 30 m/s, small deformations only occur at the outer surface of the round jet and no modification of the vorticity thickness is observed. At 40 m/s, the authority of the actuator is not significant on the time-averaged velocity at $x/D = 0.1$. The cross-stream, time-averaged fields were only measured in the near-exit region of the axisymmetric air jet, and it could be helpful to reproduce these measurements with a larger investigation field. Indeed, simultaneous acquisitions in the near- and far-field regions could confirm or refute the fact that small disturbances imparted to the jet shear layer by plasma actuation have an impact on the mixing further downstream by an amplification of the natural instabilities.

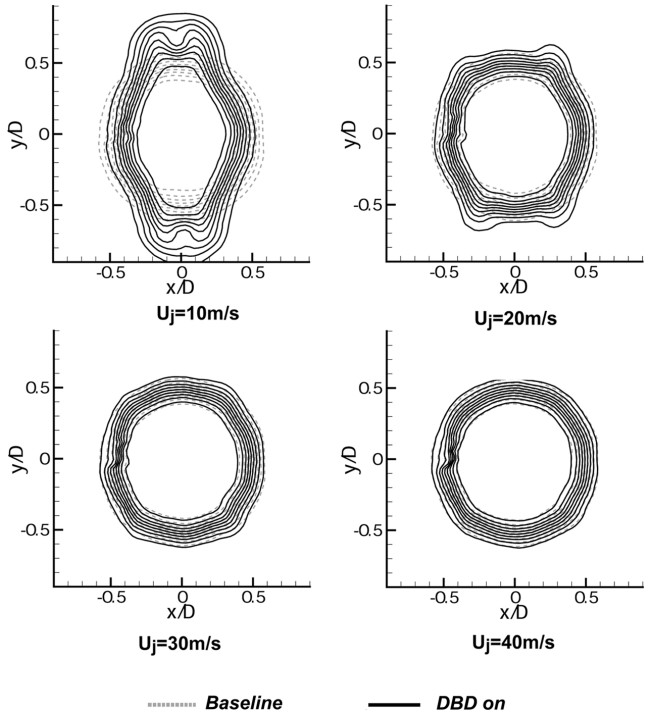

Fig. 9 Time-averaged velocity norms in transverse plane at $x/D = 0.1$.

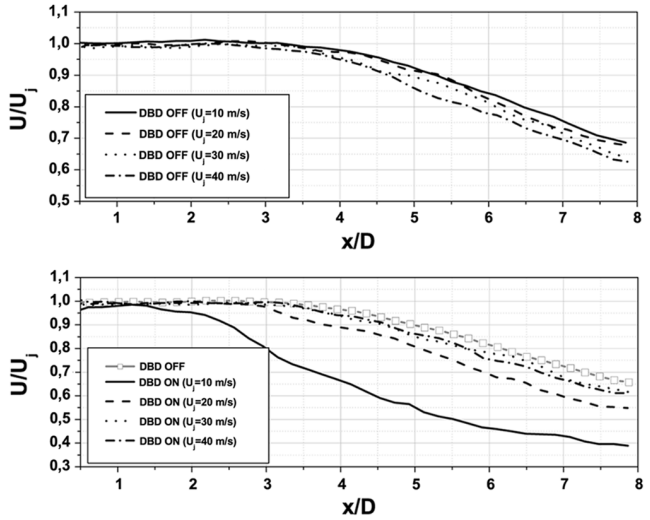

Fig. 10 Centerline velocity decay at 10, 20, 30, and 40 m/s for baseline flow and quasi-steady actuation.

C. Quasi-Steady Actuation: Characterization of the Resulted Mixing

The mixing properties of the manipulated flow can be characterized by the centerline velocity decay, by computing the turbulent kinetic energy (TKE), and by turbulent spectra. The time-averaged turbulent kinetic energy can be approached by the following expression in 2-D flows:

$$\mathrm{TKE} = \frac{1}{2}\left(\overline{u_x'^2} + \overline{u_y'^2}\right) \tag{1}$$

The jet centerline velocity decays along the x axis is plotted in Fig. 10 for the baseline and forced airflows measured by 2-D PIV. The baseline flows present a potential core ending around $x/D = 3.2$–3.5 by using the position at which the centerline velocity is equal to 99% of the jet velocity. These values are lower than the standard position of the end of the core length, but if one adds the length of the separated region upstream of the exit plane (i.e., $D/2$), then $x/D = 3.7$–4, which is close to the values obtained by Hussein et al. [34]. One can notice that centerline velocity starts decreasing at the same location whatever is the primary air jet velocity, due to the forced turbulent transition. Under actuation, the potential core is reduced by 45, 32, and 10% for a primary velocity of 10, 20, and

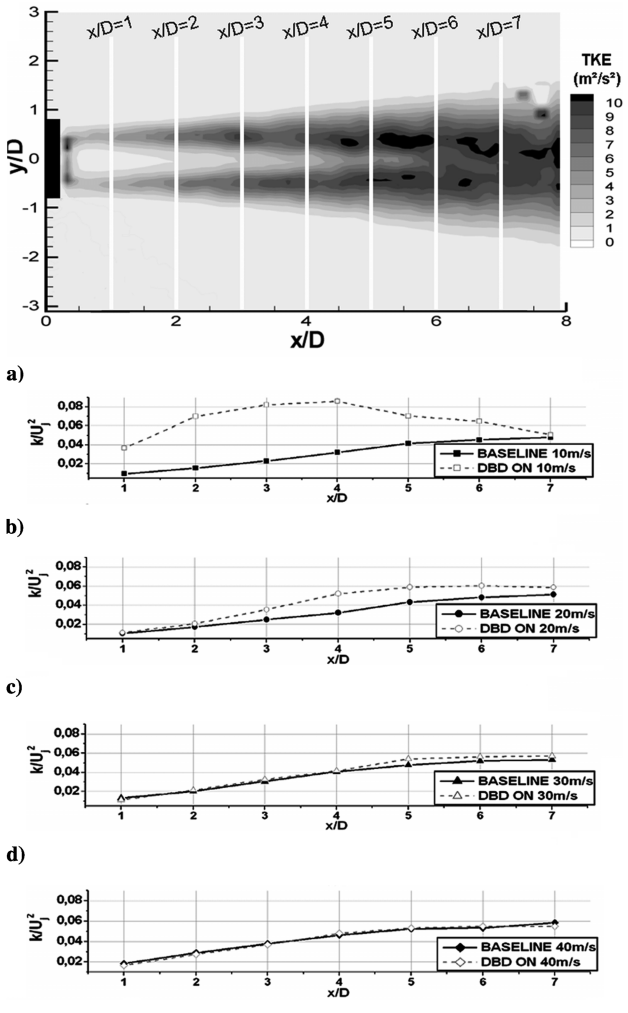

Fig. 11 Integrated value of the TKE along slices at $x/D = 1$–7 and $z/D = 0$, a) schematic view of the extraction lines and results for the primary jet velocity of b) 10, c) 20, d) 30, and e) 40 m/s.

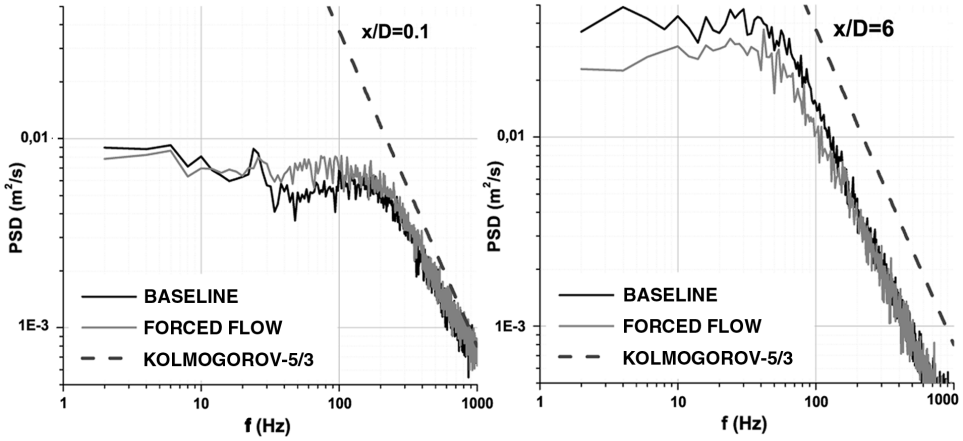

Fig. 12 Power spectra density u' along the shear layer centerline ($z/D = 0$) at $x/D = 0.1$ and $x/D = 6$ ($U_j = 20$ m/s).

30 m/s, respectively (illustrated in Fig. 10). At 40 m/s, the difference in jet centerline decay is not significant.

To characterize the entire flow, the integrated values of TKE along slices ($x/D = 1$–7 at $z/D = 0$) of the 2-D PIV fields are shown in Fig. 11a (the integration is performed over the y direction). For $U_j = 10$ and 20 m/s, illustrated in Figs. 11b and 11c, respectively, the quasi-steady actuation leads to an increase of integrated TKE over the whole range of x/D compared with the baseline flows. In particular, a maximal gain in TKE of about 156% (at $x/D = 4$) and 62% (at $x/D = 4$) can be observed for $U_j = 10$ and 20 m/s, respectively. The results at 30 m/s demonstrate that the TKE in the near-field region remains unchanged compared with the baseline case, but starts to gradually rise from the $x/D = 4$ position (TKE gain of 12% at $x/D = 5$). This particular trend may result from nonlinear interactions or 3-D effects. Indeed, the cross-stream acquisitions at 30 m/s reveal that the flow is mainly modified at the corner of the DBD electrodes, that is, at $z/D \neq 0$. Thus, it was expected that few modifications occur at $z/D = 0$ in the near-exit region. The situation differs at the end of the potential core, at which the surrounding flow structures merge at the centerline axis. The flow modifications are out of view in the near-field region but become noticeable beyond $x/D = 4$, downstream of the end of the potential core where flow modifications are highly three-dimensional. Finally, as previously suggested, no effect is observed at 40 m/s in this investigated plane, as shown in Fig. 11e.

Figure 12 shows the power density spectra measured by LDV at $x/D = 0.1$ and $x/D = 6$ along the shear layer centerline for a primary air jet velocity set to 20 m/s. In the near-field region ($x/D = 0.1$), the manipulated flow presents an increase of turbulence energy for the low frequencies ($f < 200$ Hz). The flow structures associated with frequencies between 30 and 200 Hz are energized. At 20 m/s, the initial momentum thickness θ_0 is approximately equal to 1.3 mm and the Strouhal number based on shear layer mode ($St_\theta = f\theta_0/U_c$) is 0.028 (with $f = 220$ Hz and $U_c = 10$ m/s). This value is slightly lower than the theoretical value of the Strouhal number of the most unstable mode ($St_\theta = 0.033$) defined by Gutmark and Ho [35]. The discrepancy is certainly due to the accuracy of the momentum thickness computation. Nevertheless, as expected, the extent of the inertial range is increased at $x/D = 6$ and, at both locations, the Kolmogorov $-5/3$ scaling is verified. One can note that the presence of a noise floor in the density spectra limits the accuracy of the results to the beginning of the inertial subrange. At $x/D = 6$, the spectra present large modifications of the energy distribution at the low frequencies ($f < 200$ Hz) and a turbulence energy decrease is observed. Indeed, the TKE is primarily increased compared with the baseline flow up to $x/D = 3$ and is decreased further downstream. Thus, contrary to a quasi-steady counterflow actuation, which results in a turbulence increase in the whole flowfield [32], the mixing enhancement in the near-exit region induces turbulence reduction in the far-field region [36]. The TKE distribution computed using the LDV data confirms this behavior, as presented in Fig. 13. However, further investigations are required to define which turbulent process (forced decrease of the production sources or enhancement of the dissipation terms) is responsible for the observed TKE reduction in the far-field region.

D. Unsteady Actuation: Characterization of the Resultant Mixing

Mixing enhancement is usually based on excitation of natural instabilities. A pulsed addition of momentum can act on the large-scale coherent structures existing in shear layers, and it has been recognized that unsteady manipulation of these structures could enhance the global fluid response, increase the mixing and spreading of the air jet and reduce the low-frequency noise level. Unsteady excitations are performed with a duty cycle of 50%, which halves the electrical power consumption of the control device. In this section, the control authority is evaluated by the turbulent spectra analyses and by the observations based on the evolution of the integrated TKE value over the range of investigated Strouhal values. The Strouhal number St, or reduced frequency, associated with the jet column mode is defined by

$$St = \frac{fD}{U_j}$$

Figure 14 shows the streamwise evolution of the curves of power spectra density at 20 m/s measured by LDV. Data are collected along the shear layer centerline at $x/D = 0.1$, 3, and 6 for unsteady actuation operated at frequencies f of 40, 160, and 400 Hz ($St = 0.1$, 0.4, and 1, respectively). The first result is that the turbulent energy is decreased (from $x/D = 0.1$) at each Strouhal number, contrary to the quasi-steady actuation. However, one can remark that distinct peaks of energy appear at the excitation frequency forced by the DBD actuator as previously demonstrated by Hultgren and Ashpis [37].

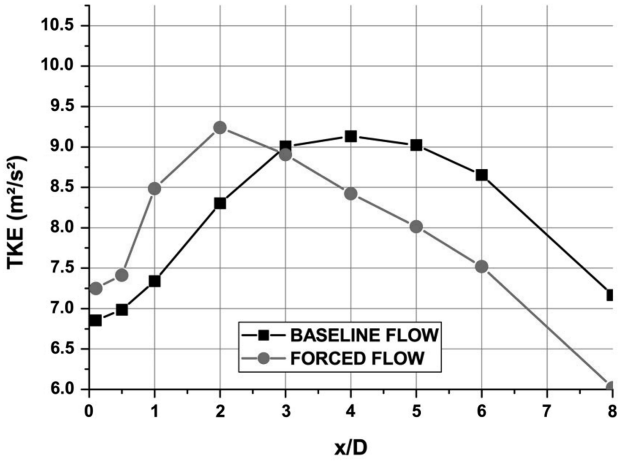

Fig. 13 Turbulent kinetic energy computed along the shear layer centerline ($z/D = 0$).

For instance, at the lower Strouhal number ($St = 0.1$, i.e., $f = 40$ Hz), energy peaks occur at 40 Hz, as well as at its three higher-order harmonics, as shown in Fig. 14. These energy peaks are consistent with the time-averaged phase acquisition (see Sec. III.A), which have demonstrated that a vortex shedding occurs along the bevel. The peaks of energy also demonstrate that the vortex shedding is forced at the excitation frequency, and it is expected that, for pulsate actuation, trains of vortices are shed from the jet exhaust. At $St = 0.1$, the intensity of the peaks remains constant with the distance to the shear layer origin. Then, there is no energy absorption at this frequency, however, the ratio between the peaks of energy and the overall energy is decreased along the shear layer centerline. Actuation at a reduced frequency above $St = 0.4$ lost in some degree its capacity to manipulate the flow structures in the near-field and far-field regions. Nevertheless, an interesting event occurs at the jet exit for $St = 1$ (at $x/D = 0.1$): the spectrum presents a small energy peak at $f = 400$ Hz and its third subharmonic, highlighting a plausible vortex merging process for this forced regime.

According to Fig. 14, the most effective modification in the structure organization occurs for the unsteady actuation at a reduced frequency of 0.1. Other Strouhal numbers are investigated by LDV and the spectra at $x/D = 3$ for excitation at $St = 0.05$, 0.1, 0.2, 0.4, 0.8, and 1 ($f = 20$, 40, 80, 160, 320, and 400 Hz, respectively) are plotted in Fig. 15. The spectra confirm that excitation at the low reduced frequency ($St < 0.4$) induce the most effective turbulence modification in the shear layer. The TKE values computed along the shear layer centerline confirm this observation. Indeed, above $St = 0.4$ in Fig. 15, the TKE distribution presents a similar shape and low magnitude, whereas a lower reduced excitation frequency (i.e., $St < 0.2$) results in a significant increase in TKE. It is speculated that the airflow produced by the actuator is similar over the investigated frequency range and fluid considerations could explain the observed frequency limitation. Above $St = 0.4$ ($f > 160$ Hz), the excitation produces large-scale structures in the near-field region, but these structures rapidly disappear further downstream, as illustrated in Figs. 14 and 15. At these frequencies, it could be expected that the size of the induced flow structures is smaller and corresponds to the inertial region. This region is associated with a rise of the turbulent cascade and turbulent dissipation, which could rapidly absorb the generated vortices. For instance, at $St = 0.1$, the peak of energy and its harmonics are visible up to $x/D = 3$. Further downstream, the inertial region is shifted down due to the enlargement of the mixing layer and the increase in δ_w (at $x/D = 6$, the inertial region starts approximately at $f = 60$ Hz). At $x/D = 6$, the harmonics of the input frequency occur in the inertial region and may be absorbed due to higher dissipation or loss of energy, resulting from the nonlinear interactions occurring at high-excitation modes. This concept could explain the reduction of the control efficiency when an excitation frequency greater than the beginning of the inertial zone is applied to the jet. However, an excitation of the flow structures at $St = 0.2$ appears to be particularly efficient to increase the turbulence in the near-exit region, as demonstrated in Fig. 16. Contrary to the case of $St = 0.2$, one can remark that actuation at the lower frequencies (i.e., $St = 0.05$ and 0.1) induces a turbulent increase up to $x/D = 8$. Finally, an increase of turbulence over the whole shear layer is realized by exciting the flow with a low frequency (i.e., $St = 0.05$ and 0.1), whereas an excitation at $St = 0.2$ increases the turbulence in the near shear layer region, while the TKE is decreased further downstream. The comparison of the baseline flow, quasi-steady, and unsteady forcing also indicates that unsteady actuation at low reduced frequency (i.e., $St < 0.2$) is more effective than the quasi-steady one shown in Fig. 17. As shown in Fig. 18 by 2-D PIV, the turbulent kinetic energy is largely increased when an unsteady actuation is performed while there is no major flow change on the

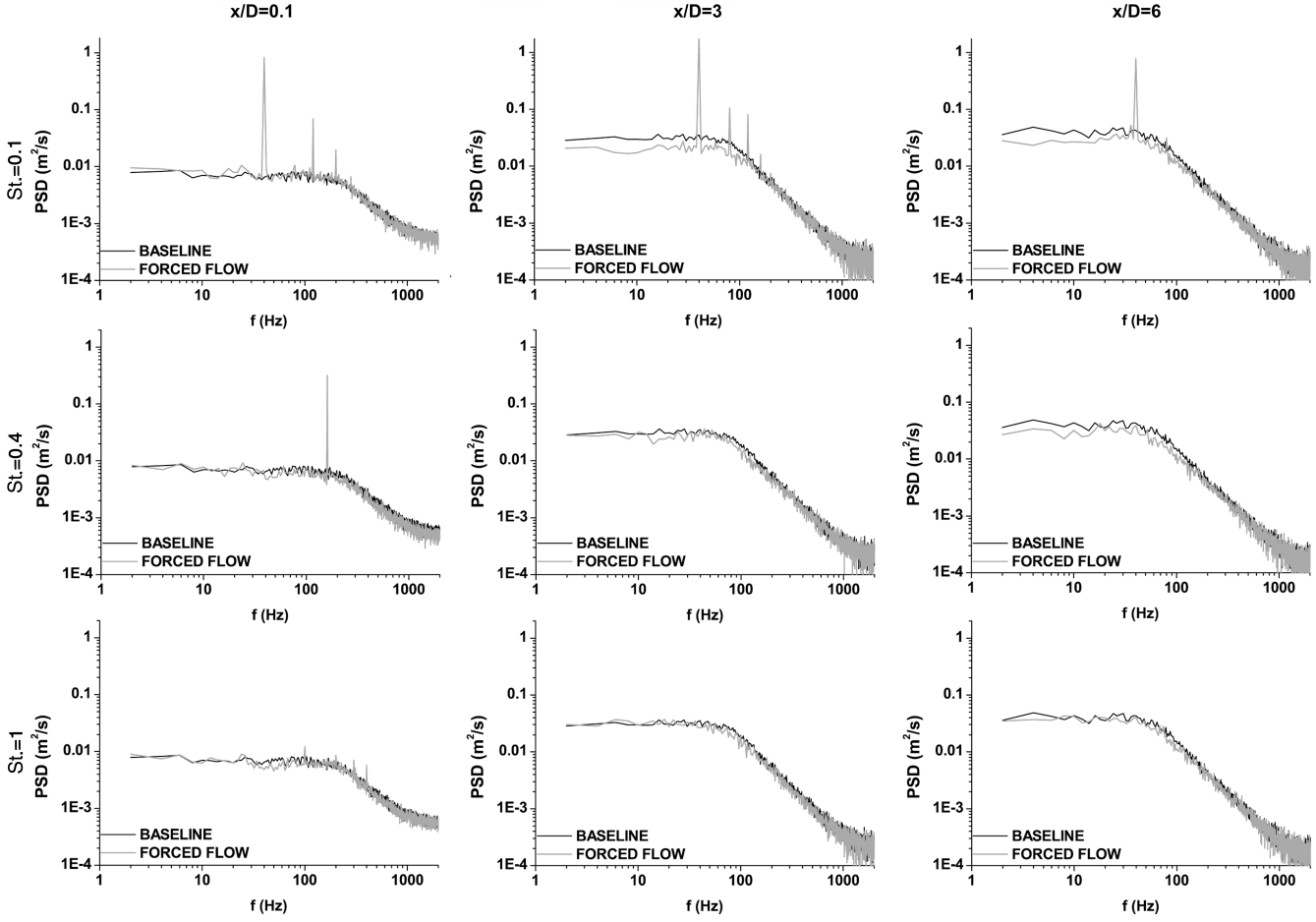

Fig. 14 Power spectra density u' along the shear layer centerline at $x/D = 0.1$, 3, and 6 ($U_j = 20$ m/s) for unsteady actuation at a reduced frequency $St = 0.1$, 0.4, and 1.

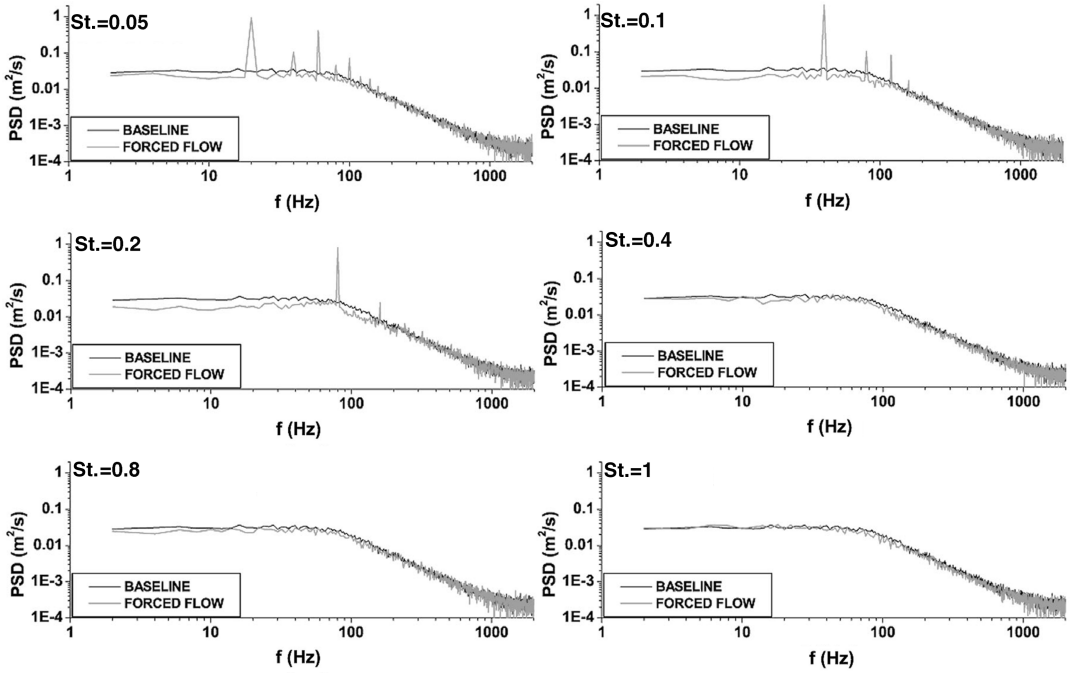

Fig. 15 Power spectra density u' along the shear layer centerline at $x/D = 3$ ($U_j = 20$ m/s) for unsteady actuation at a reduced frequency of 0.05, 0.1, 0.2, 0.4, 0.8, and 1.

time-averaged velocity norm compared to a quasi-steady actuation. The rise in TKE could result from the modification of the instantaneous velocities. Indeed, as illustrated in Fig. 18, it seems that the unsteady actuation produces a velocity contraction downstream of the jet exit, resulting in successive "puffs" of velocity. Further analysis is required to quantify this flow particularity, but it seems reasonable to assume that the flow contraction results from two large-scale structures produced on each side of the jet by the unsteady actuation, as highlighted by the phase-averaged PIV fields.

Complementary to the TKE evolution along the centerline of the shear layer and the comparison of quasi-steady and unsteady forcing, the PIV fields are used to compute the integrated TKE values on slices at $x/D = 1$–4 for velocities of 20 and 30 m/s only, as previously mentioned. This integrated quantity is suitable to inspect the TKE value over the whole flow slice. More, this quantity could highlight an optimal excitation frequency differing from the estimation based on the computation of TKE at a discrete acquisition point. The results plotted in Fig. 19 suggest that the integrated TKE is increased when the flow is forced at a Strouhal number around 0.25–0.32. One can note that this trend is emphasized along the centerline axis. This range of Strouhal values reasonably agrees with the literature about the preferred frequency of the jet column instability [38] and suggests that the nonthermal actuator can interact with the jet column instability mode. At each investigated case, the integrated TKE value is significantly enhanced when an unsteady actuation is performed comparatively to a quasi-steady one. In particular, the turbulence gain is about 78% at 30 m/s, whereas the turbulent energy is increased to 49% at 20 m/s. According to the results arising from the turbulent spectra, it could be suspected that this increase in the turbulent state results from a periodic shedding or trains of large-scale flow structures that occur when a pulsing excitation is applied. However, a reduced excitation frequency above 0.9 has limited effects in increasing the TKE, as demonstrated in Fig. 19 at 20 m/s. Additional measurements are now required to describe the interaction between the weakly ionized plasma surface and the external flow. In particular, the capability of such actuator to promote creation of large-scale structures requires a new experiment to establish a possible relationship between the excitation frequency and the size and strength of the produced vortices. Indeed, such

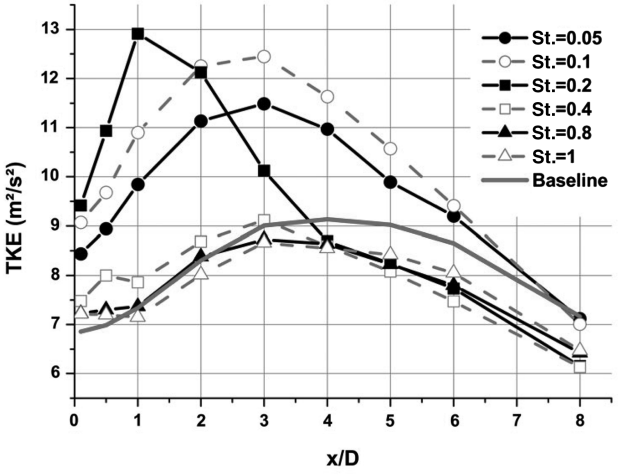

Fig. 16 TKE values computed along the shear layer centerline (at $z/D = 0$) for unsteady actuation at $U_j = 20$ m/s.

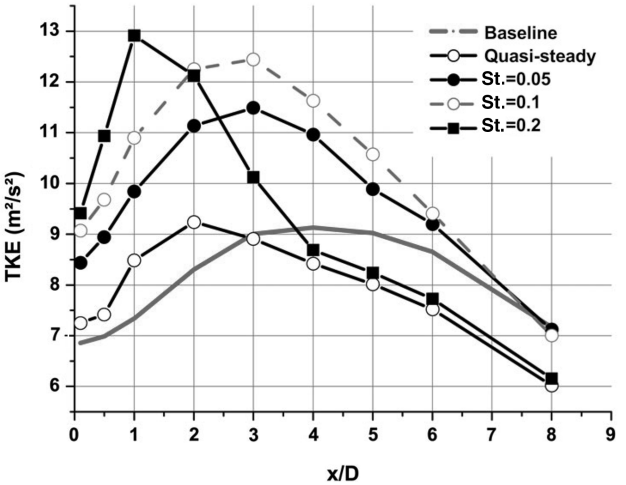

Fig. 17 Comparison of TKE values at $z/D = 0$ along the shear layer centerline for baseline, quasi-steady, and unsteady forcing.

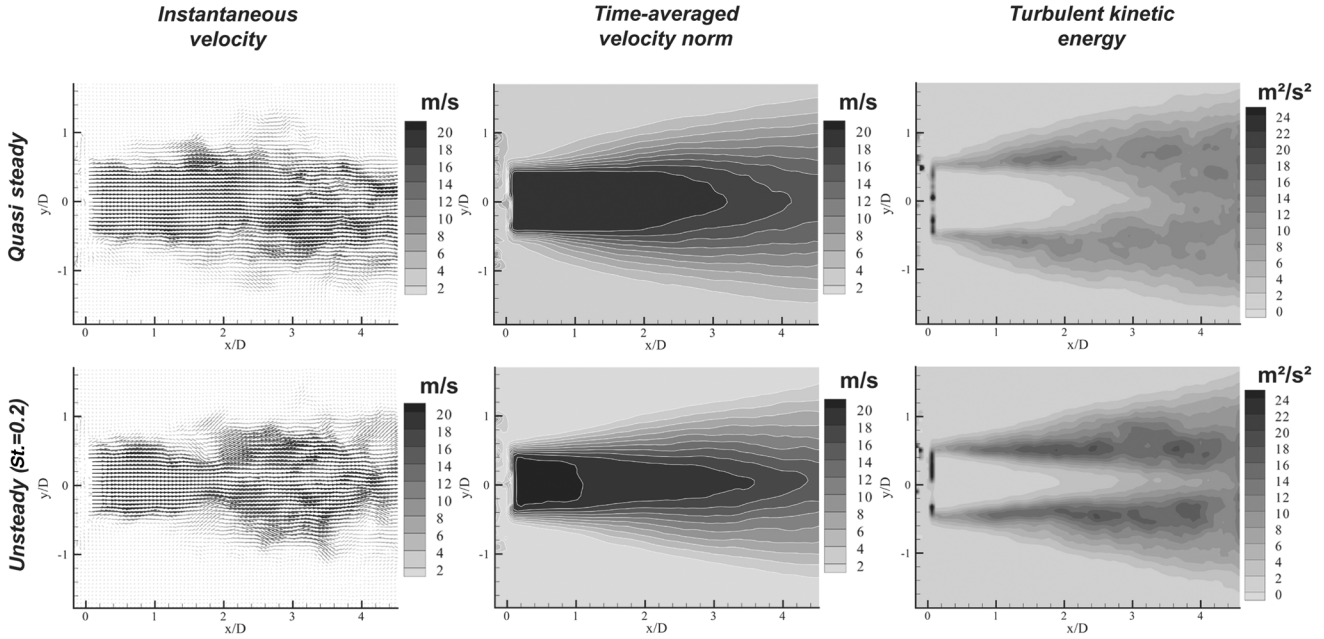

Fig. 18 Instantaneous velocity, time-averaged norm, and turbulent kinetic energy at $z/D = 0$ for quasi-steady and unsteady ($St = 0.2$) actuation for a freestream velocity U_j of 20 m/s.

capability may suggest that a DBD actuator can control the turbulent scales.

IV. Conclusions

An active control device composed of two nonthermal plasma actuators is combined with a passive diffuser to enhance the mixing of a free shear layer, resulting from a turbulent axisymmetric jet exhausting in surrounding airflow at rest. Spatial measurements by PIV and stereoscopic PIV, or temporal data acquired by an LDV system, are used to study the effects of steady and unsteady actuations on the main characteristics of the free jet. The effects of the weakly ionized region on the potential core length, the evolution of the turbulent kinetic energy, and the turbulent spectra along the

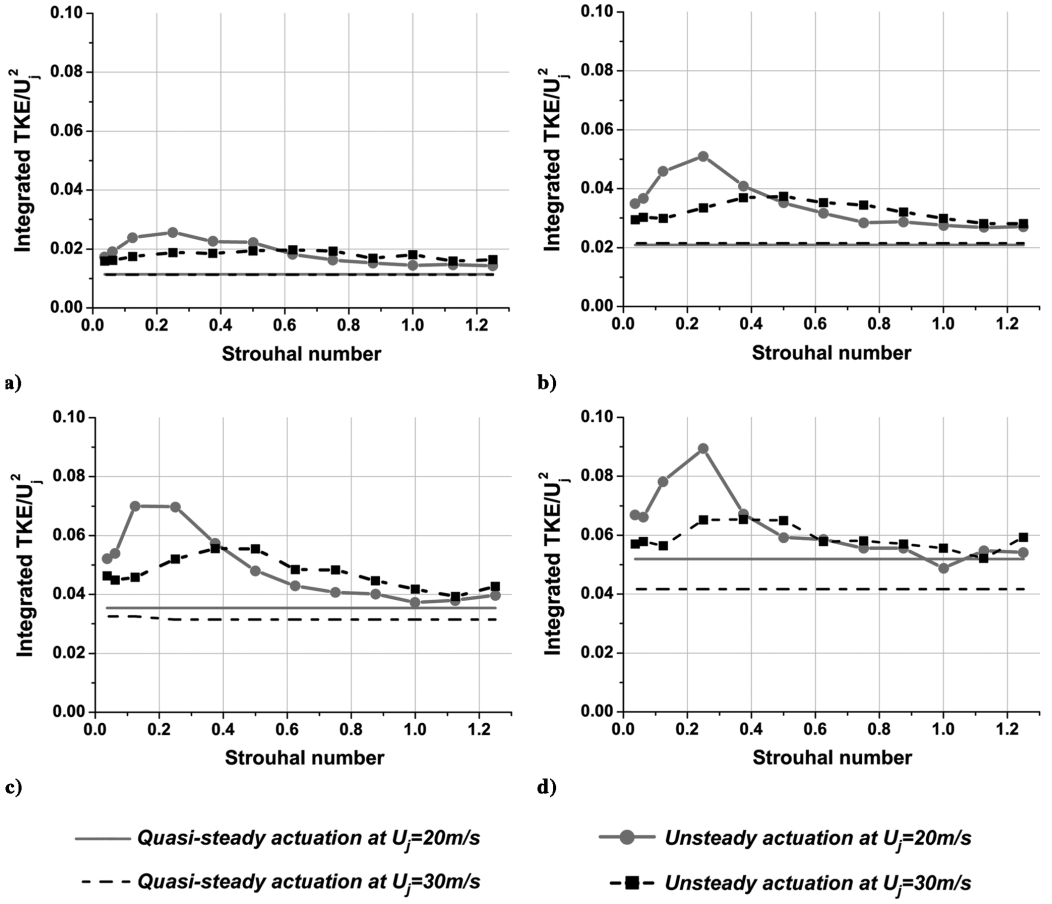

Fig. 19 Integrated TKE ($z/D = 0$) at a) $x/D = 1$, b) 2, c) 3, and d) 4 for primary air jet velocity of 20 m/s and 30 m/s.

centerline shear layer are introduced in the present paper. The authority of the actuator is investigated for primary jet velocities from 10 to 40 m/s.

Each DBD actuator produces a local flow arising from momentum transfer from the charged particles to the neutral ones. The PIV measurements inside the jet nozzle demonstrate that this local flow is used to fully reattach the naturally separated flow for an air jet velocity of 10 m/s (or partially attached the flow at $U_j = 20$ m/s). However, the vorticity thickness is increased despite of the flow reattachment, which results in a large mixing enhancement due to the increase in mixing surface and local vorticity. The time-averaged phase acquisitions establish that a shedding of coherent structures occurs at the jet exit for 10 and 20 m/s, the convective velocity being half of the centerline jet velocity, as commonly reported. The shedding of vortices is confirmed by the spectra issued from the LDV acquisitions, and the results suggest that the shedding frequency is dictated by the frequency applied to the DBD actuators. Limited results are observed for a Strouhal number above 0.4 (excitation frequency inside the inertial zone) and it seems that the small-scale structures dissipate the vortices induced by the actuation for these excitation regimes. At 40 m/s, the EFD forces produced by the actuators are supposed to be mainly used to control the dynamics of the large eddies initiated at the beginning of the diffuser. At this jet velocity, the PIV fields show that there is no significant flow modification in the streamwise and cross-stream planes at $z/D = 0$.

These results demonstrate that this configuration is effective to increase the mixing for velocity up to 30 m/s by an increase in mixing surface (at $U_j = 10$ and 20 m/s) combined with an increase in local vorticity thickness (up to 30 m/s). Under quasi-steady actuation, the core length is shortened and the integrated TKE values are increased. In the shear layer region, the TKE is increased in the near-field region ($x/D = 3$) and reduced further downstream. Under unsteady actuation, the turbulent spectra and the integrated TKE demonstrate that the most significant mixing is performed using an actuation at a reduced frequency of 0.3, this value corresponding to the jet preferred mode previously described in the literature. At this frequency, the TKE value along the shear layer centerline is characterized by a rise of turbulence in the near-exit region associated with a turbulence reduction further downstream. Actuation below this value promotes a turbulence increase up to the far-field region.

New experiments are now required to demonstrate that this actuator system is effective at higher Reynolds numbers by increasing the electric power supplied to the DBD system and by analyzing the overall manipulated flow behavior. In particular, additional cross-stream visualizations in the far-field region and PIV acquisitions along the z direction are required due to the asymmetric flow resulting from the flow controlled by the present plasma configuration. Another way consists in the use of a combination of an optimized passive diffuser shape in conjunction with a more effective plasma actuator configuration. Future investigations are also necessary to qualify the aeroacoustic near- and far-field regions.

References

[1] Kibens, V., Dorris, J., Smith, D. M., and Mossman, M. F., "Active Flow Control Technology Transition: The Boeing Ace Program," AIAA Paper 1999-3507, 1999.

[2] Lord, W. K., MacMartin, D. G., and Tillman, T. G., "Flow Control Opportunities in Gas Turbine Engines," AIAA Paper 2000-2234, 2000.

[3] Bridges, J., Wernet, M., and Brown, C., "Control of Jet Noise Through Mixing Enhancement," NASA Rept. 2003-212335, 2003.

[4] Laurendeau, E., Bonnet, J. P., Jordan, P., and Delville, J., "Impact of Fluidic Chevrons on the Turbulence Structure of a Subsonic Jet," AIAA Paper 2006-3510, 2006.

[5] Lardeau, S., Lamballais, E., and Bonnet, J. P., "Direct Numerical Simulation of a Jet Controlled by Fluid Injection," *Journal of Turbulence*, Vol. 3, No. 2, 2002, pp. 1–25. doi:10.1088/1468-5248/3/1/002

[6] Corke, T. C., and Kusek, S. M., "Resonance in Axisymmetric Jets with Controlled Helical Mode Input," *Journal of Fluid Mechanics*, Vol. 249, 1993, pp. 307–336. doi:10.1017/S0022112093001193

[7] Zaman, K., Reeder, M., and Samimy, M., "Control of an Axisymmetric Jet Using Vortex Generators," *Physics of Fluids*, Vol. 6, No. 2, 1994, pp. 778–793. doi:10.1063/1.868316

[8] Huerre, P., and Monkewitz, P. A., "Local and Global Instabilities in Spatially Developing Flows," *Annual Review of Fluid Mechanics*, Vol. 22, Jan. 1990, pp. 473–537. doi:10.1146/annurev.fl.22.010190.002353

[9] Parekh, D. E., Kibens, V., Glezer, A., Wiltze, J. M., and Smith, D. M., "Innovative Jet Flow Control: Mixing Enhancement Experiments," AIAA Paper 96-0308, 1996.

[10] Corke, T. C., and Post, M. L., "Overview of Plasma Flow Control: Concepts, Optimization and Applications," AIAA Paper 2005-563, 2005.

[11] Moreau, E., "Airflow Control by Non-Thermal Plasma Actuators," *Journal of Physics D: Applied Physics*, Vol. 40, No. 3, 2007, pp. 605–636. doi:10.1088/0022-3727/40/3/S01

[12] Sosa, R., Artana, G., Moreau, E., and Touchard, G., "Stall Control at High Angle of Attack with Plasma Sheet Actuators," *Experiments in Fluids*, Vol. 42, No. 1, 2007, pp. 143–167. doi:10.1007/s00348-006-0227-5

[13] Corke, T. C., He, C., and Patel, M. P., "Plasma Flaps and Slats: An Application of Weakly Ionized Plasma Actuators," AIAA Paper 2004-2127, 2004.

[14] Artana, G., Sosa, R., Moreau, E., and Touchard, G., "Control of the Near-Wake Flow Around a Circular Cylinder with Electrohydrodynamic Actuators," *Experiments in Fluids*, Vol. 35, No. 6, 2003, pp. 580–588. doi:10.1007/s00348-003-0704-z

[15] McLaughlin, T. E., Felker, B., and Avery, J. C., "Further Experiments in Cylinder Wake Modification with Dielectric Barrier Discharge Forcing," AIAA Paper 2006-1409, 2006.

[16] Grundmann, S., and Tropea, C., "Experimental Transition Delay Using Glow-Discharge Plasma Actuators," *Experiments in Fluids*, Vol. 42, No. 4, 2007, pp. 653–657. doi:10.1007/s00348-007-0256-8

[17] Roth, J. R., "Electrohydrodynamically Induced Airflow in a One Atmosphere Uniform Glow Discharge Surface Plasma," *Proceeding of the 25th IEEE International Conference Plasma Science*, Inst. of Electrical and Electronic Engineers, New York, 1998, p. 291. doi:10.1109/PLASMA.1998.677891

[18] Enloe, C. L., Thomas, E., McLaughlin, T. E., VanDyken, R. D., and Kachner, K. D., "Mechanisms and Responses of a Single Dielectric Barrier Plasma," AIAA Paper 2003-1021, 2003.

[19] Pons, J., Moreau, E., and Touchard, G., "Asymmetric Surface Barrier Discharge in Air at Atmospheric Pressure: Electric Properties and Induced Airflow Characteristics," *Journal of Physics D: Applied Physics*, Vol. 38, No. 19, 2005, pp. 3635–3642. doi:10.1088/0022-3727/38/19/012

[20] Samimy, M., Kim, J., Kastner, J., Adamovich, I., and Utkin, Y., "Active Control of High-Speed and High Reynolds Number Jets Using Plasma Actuators," *Journal of Fluid Mechanics*, Vol. 578, 2007, pp. 305–330. doi:10.1017/S0022112007004867

[21] Corke, T. C., and Matlis, E., "Phased Plasma Arrays for Unsteady Flow Control," AIAA Paper 2000-2323, 2000.

[22] Benard, N., Jolibois, J., Forte, M., Touchard, G., and Moreau, E., "Control of an Axisymmetric Subsonic Air Jet by Plasma Actuator," *Experiments in Fluids*, Vol. 43, No. 4, 2007, pp. 603–616. doi:10.1007/s00348-007-0344-9

[23] Forte, M., Jolibois, J., Moreau, E., Touchard, G., and Cazalens, M., "Optimization of a Dielectric Barrier Discharge Actuator by Stationary and Non- Stationary Measurements of the Induced Flow Velocity: Application to Airflow Control," AIAA Paper 2006-2863, 2006.

[24] Post, M. L., and Corke, T. C., "Separation Control Using Plasma Actuators: Stationary and Oscillating Airfoils," AIAA Paper 2004-0841, 2004.

[25] Albrecht, H. E., Borys, M., Damasche, N., and Tropea, C., "Laser Doppler and Phase Doppler Measurement Techniques," Springer–Verlag, Berlin, 2003, pp. 1–738.

[26] van Maanen, H. R. E., Nobach, H., and Benedict, L. H., "Improved Estimator for the Slotted Autocorrelation Function of Randomly Sampled LDA Data," *Measurement Science and Technology*, Vol. 10, No. 1, 1999, pp. L4–L7. doi:10.1088/0957-0233/10/1/002

[27] Benedict, L. H., and Gould, R. D., "Towards Better Uncertainty Estimates for Turbulence Statistics," *Experiments in Fluids*, Vol. 22, No. 2, 1996, pp. 129–136.

doi:10.1007/s003480050030
[28] Kerherve, F., Jordan, P., Gervais, Y., Valiere, J. C., and Braud, P., "Two-Point Laser Doppler Velocimetry Measurements in a Mach 1.2 Cold Supersonic Jet for Statistical Aeroacoustic Source Model," *Experiments in Fluids*, Vol. 37, No. 3, 2004, pp. 419–437. doi:10.1007/s00348-004-0815-1
[29] Benedict, L. H., Nobach, H., and Tropea, C., "Benchmark Tests for the Estimation of Power Spectra from LDA Signals," *Proceedings of the 9th International Symposium on Application of Laser Technology to Fluid Mechanics*, Vol. 1, Inst. Superior Tecnico Paper 32.6, July 1998.
[30] Gregory, J. W., Ruotolo, J. C., Byerley, A. R., and Mclaughlin, T. E., "Switching Behavior of a Plasma-Fluidic Actuator," AIAA Paper 2007-785, 2007.
[31] Benard, N., Braud, P., Touchard, G., and Moreau, E., "Detachment and Attachment of an Axisymmetric Turbulent Airjet: Control by Plasma Actuator," *Experimental Thermal and Fluid Science*, Vol. 32, No. 6, 2008, pp. 1193–1203.
[32] Benard, N., Braud, P., Pons, J., Touchard, G., and Moreau, E., "Quasi-Steady and Unsteady Actuation by Surface Nonthermal Plasma Discharge for Control of a Turbulent Round Air Jet," *Journal of Turbulence*, Vol. 8, No. 49, 2007, pp. 1–24. doi:10.1080/14685240701656139
[33] Zaman, K. B. M. Q., Samimy, M., and Reeder, M. F., "Effect of Tabs on the Evolution of an Axisymmetric Jet," NASA Rept. NASA-TM-104472, 1991.
[34] Hussein, J. H., Capp, S. P., and George, W. K., "Velocity Measurements in a High-Reynolds Number, Momentum Conserving, Axisymmetric, Turbulent Jet," *Journal of Fluid Mechanics*, Vol. 258, 1994, pp. 31–75. doi:10.1017/S002211209400323X
[35] Gutmark, E., and Ho, C. M., "Preferred Modes and the Spreading Rates of Jets," *Physics of Fluids*, Vol. 26, No. 10, 1983, pp. 2932–2938. doi:10.1063/1.864058
[36] Laurendeau, E., Bonnet, J. P., Jordan, P., and Delville, J., "Turbulence Jet Noise Control by Fluid Chevrons," *Proceedings of 4th Turbulent and Shear Flow Phenomena* NASA Paper No. 32, June 2005.
[37] Hultgren, L. S., and Ashpis, D. E., "Demonstration of Separation Delay with Glow-Discharge Plasma Actuators," AIAA Paper 2003-1025, 2005.
[38] Crow, S. C., and Champagne, F. H., "Orderly Structure in Jet Turbulence," *Journal of Fluid Mechanics*, Vol. 48, 1971, pp. 547–591. doi:10.1017/S0022112071001745

N. Clemens
Associate Editor